Cellular/Molecular

Rabconnectin3α Promotes Stable Activity of the H^+ Pump on Synaptic Vesicles in Hair Cells

Zev Einhorn, Josef G. Trapani, Qianyong Liu, and Teresa Nicolson

Oregon Hearing Research Center and Vollum Institute, Howard Hughes Medical Institute, Oregon Health and Science University, Portland, Oregon 97239

Acidification of synaptic vesicles relies on the vacuolar-type ATPase (V-ATPase) and provides the electrochemical driving force for neurotransmitter exchange. The regulatory mechanisms that ensure assembly of the V-ATPase holoenzyme on synaptic vesicles are unknown. Rabconnectin3α (Rbc3α) is a potential candidate for regulation of V-ATPase activity because of its association with synaptic vesicles and its requirement for acidification of intracellular compartments. Here, we provide the first evidence for a role of Rbc3α in synaptic vesicle acidification and neurotransmission. In this study, we characterized mutant alleles of *rbc3α* isolated from a large-scale screen for zebrafish with auditory/vestibular defects. We show that Rbc3α is localized to basal regions of hair cells in which synaptic vesicles are present. To determine whether Rbc3α regulates V-ATPase activity, we examined the acidification of synaptic vesicles and localization of the V-ATPase in hair cells. In contrast to wild-type hair cells, we observed that synaptic vesicles had elevated pH, and a cytosolic subunit of the V-ATPase was no longer enriched in synaptic regions of mutant hair cells. As a consequence of defective acidification of synaptic vesicles, afferent neurons in *rbc3α* mutants had reduced firing rates and reduced accuracy of phase-locked action potentials in response to mechanical stimulation of hair cells. Collectively, our data suggest that Rbc3α modulates synaptic transmission in hair cells by promoting V-ATPase activity in synaptic vesicles.

Introduction

The hair cell is the sensory mechanoreceptor of the auditory and vestibular organs, as well as the lateral-line organ in fish and amphibians. Hair cells transduce stimuli such as sound, head movements, and changes in water currents into electrical signals. Depolarization of the hair-cell receptor potential results in the release of synaptic vesicles containing the neurotransmitter glutamate at the basal end of the cells. Forward genetic screens for hearing and balance mutants in zebrafish and mouse knock-outs have identified several of the molecules important for synaptic transmission in hair cells (Nicolson et al., 1998; Leibovici et al., 2008; Obholzer et al., 2008; Trapani et al., 2009). One such protein is vesicular glutamate transporter 3 (Vglut3), which loads neurotransmitter into synaptic vesicles by exchanging protons for glutamate (Fremeau et al., 2002; Obholzer et al., 2008; Ruel et al., 2008; Seal et al., 2008). Protons are concentrated into the lumen of the synaptic vesicle by the vacuolar-type ATPase (V-ATPase), and as a result, robust V-ATPase activity is critical for proper synaptic transmission (Schenck et al., 2009; Goh et al., 2011). However, relatively little is known about how synaptic vesicles acquire the V-ATPase in its fully assembled and active state.

The V-ATPase holoenzyme is a complex that contains a cytosolic (V1) sector and a membrane (V0) sector that are each composed of multiple subunits. The cytosolic and membrane sectors are essentially preassembled and can reversibly disassociate (Smardon et al., 2002; Trombetta et al., 2003; Smardon and Kane, 2007). Regulated assembly of the V-ATPase holoenzyme is an efficient mechanism for modulating V-ATPase activity (Toei et al., 2010). Whether regulated holoenzyme assembly also shapes V-ATPase activity on synaptic vesicles is unknown.

Rabconnectin3α (Rbc3α) is a potential candidate for regulating the assembly of the V-ATPase holoenzyme on synaptic vesicles for several reasons. Recent work has shown that the Rbc3 complex (composed of Rbc3α and Rbc3β) is essential for acidification of intracellular compartments in *Drosophila* ovarian tissue and mammalian cell lines (Yan et al., 2009; Sethi et al., 2010). Moreover, Rbc3β biochemically interacts with insect V1 subunits E and H, as evidenced by coimmunoprecipitation experiments (Yan et al., 2009). Previous evidence also supports a role in synaptic vesicle function for the Rbc3 complex: Rbc3α and Rbc3β subunits were originally identified from purified synaptic vesicle fractions and antibodies against Rbc3α-labeled synaptic regions of the rat hippocampus (Nagano et al., 2002; Kawabe et al., 2003). Together, these data raise the possibility that the Rbc3 complex modulates V-ATPase activity on synaptic vesicles by promoting holoenzyme assembly.

In this study, we examined the morphology and activity of hair-cell synapses of *rbc3α* mutant zebrafish to determine the

Received April 6, 2012; revised June 12, 2012; accepted June 22, 2012.

Author contributions: Z.E., J.G.T., Q.L., and T.N. designed research; Z.E., J.G.T., Q.L., and T.N. performed research; Z.E., J.G.T., and Q.L. analyzed data; Z.E., J.G.T., and T.N. wrote the paper.

This study was supported in part by National Institutes of Health Grant R01 DC006880. We thank the members of the Tübingen 2000 Screen Consortium for their assistance in isolating the *rbc3α* alleles.

Correspondence should be addressed to Teresa Nicolson, Howard Hughes Medical Institute, Oregon Hearing Research Center and Vollum Institute, 3181 SW Sam Jackson Park Road, Oregon Health and Science University, Portland, OR 97239. E-mail: nicolson@ohsu.edu.

J. G. Trapani's present address: Department of Biology and Neuroscience Program, Amherst College, Amherst, MA 01002.

Q. Liu's present address: Bioanalysis-US, Drug Metabolism Research Laboratories, Astellas Pharma Global Development, 8045 Lamon Avenue, Skokie, IL 60077.

DOI:10.1523/JNEUROSCI.1705-12.2012

 0270-6474/12/3211144-13$15.00/0

function of Rbc3α in hair cells. Our observations indicate that *rbc3α* mutant hair cells have overall normal synaptic structure, but synaptic vesicles fail to fully acidify presumably because of fewer assembled V-ATPase holoenzymes. We propose that Rbc3α plays a role in modulating vesicular V-ATPase activity in hair cells that ultimately affects proper synaptic transmission that is essential for both auditory and vestibular function.

Materials and Methods

Fish strains. Wild-type (WT), mutant, and transgenic larvae were maintained in both Tübingen and Top Long Fin strains. Larvae were kept at 28.5°C in the dark in E3 buffer during development. Mutants were identified in a large-scale ethyl-*N*-nitrosourea screen (Tübingen 2000 Screen Consortium). Both sexes were examined.

Molecular biology. For determination of alleles, mRNA was extracted from day 5 zebrafish larvae by standard methods. First-strand cDNA was generated from transcripts with the SuperScript III First-Strand Synthesis System (Invitrogen). Partial *rbc3α* ds-cDNAs were generated by PCR using primers targeting first (ATG-4551 bp) and second (4222–9105 bp) halves of the predicted full-length transcript (forward primer, 5′-atgcatctgcaccaggtgctgacggg-3′; reverse primer, 5-cacctgtgcatgttcggg-3; forward primer, 5′-gttgccggtcgagatggtggacg-3; reverse primer, 5-ttagaggatctggaatatactggccg-3) and were sequenced with internal primers.

Full-length *rbc3α* (GenBank accession number is pending) was generated by TA cloning both halves of ds-cDNAs into TOPO 2.1 PCR vectors (Invitrogen), restriction-enzyme digestion with AgeI and NotI enzymes (New England Biolabs), and religation of fragments with T4 DNA Ligase (New England Biolabs).

Expression constructs were generated with Multisite Gateway Technology (Invitrogen; Kwan et al., 2007). In brief, full-length *rbc3α* (ATG-9105) was PCR amplified with Gateway-compatible attB sites (forward primer, 5′-ggggacagctttcttgtacaaagtggccatgcatctgcaccaggtgctgacggg-3; reverse primer, 5- ggggacaactttgtataataaagttgcttagaggatctggaatatactggccg-3) and recombined to generate 3′ entry vector *p3E–rbc3α*, then *p3E–rbc3α* was recombined with *p5E–6.5myosin6b* minimal promoter (Mo and Nicolson, 2011), *pME–GFP*, and the *pDestination 395* vector to generate *−6.5kb_myosin6b:gfp–rbc3α;clcm2:gfp*. In a similar manner, *atp6v1aa* contained in the *pME18S–FL3* (American Type Culture Collection) was PCR amplified with primers (forward primer, 5-ggggacaagtttgtacaaaaaagcaggctccgccacca tggatttttccaagctgcctaagatccga-3′; reverse primer, 5-ggggaccactttgtacaagaaagctgggtcgtcttccagggtgcggaaggaattctg-3) and recombined with *pME. atp6v0a1* contained in the *pME18S–FL3* (ATCC) was PCR amplified with primers (forward primer, 5′- ggggacagctttcttgtacaaagtggcgatgggggagctgtttcgcagcgagg-3′; reverse primer, 5-ggggacaactttgtataataaagttgcttattcttca gacttgccatccaga-3) and recombined with *p3E. pME–atp6v1aa* and *p3E–atp6v0a1* were cloned to generate *−6.5myosin6b:atp6v1aa–GFP,clcm2:GFP* and *−6.5myosin6b:GFP–atp6v0a1,clcm2:GFP* constructs, respectively. Constructs were then microinjected (50 ng/μl) along with *Tol2* transposase mRNA at the one-cell stage of embryos.

Generation of transgenic strains. Rbc3α$^{+/Q850X}$ animals were in-crossed and microinjected with *Tol2* mRNA and *−6.5myosin6b:atp6v1aa–gfp; clcm2:gfp*. F0 animals were screened and crossed to *rbc3α*^{Q850X} to generate F1 transgenic animals *Tg(−6.5myosin6b:atp6v1aa–gfp,clcm2:gfp); rbc3α*^{Q850X}.

In situ *hybridization.* Digoxygenin-labeled riboprobes were generated with the DIG Labeling Kit (Roche) from a previously published *rbc3α* probe, CB952 (Thisse et al., 2001). *In situ* hybridization was performed as described previously (Söllner et al., 2004) with 200 ng of probe. Larvae at 72 h postfertilization were imaged as whole mounts. Larvae at 4 d postfertilization (dpf) were cryosectioned into 12 μm slices using standard methods. Larvae were viewed on a Carl Zeiss Axio bright-field microscope using either a 10× or 20× dry lens objective. Images were captured with an AxioCam MRc5 color digital camera using Axiovision software and exported as TIFF files to Adobe Photoshop or NIH ImageJ for analysis.

RT-PCR of neuromasts and yolk epithelium. Neuromasts along the head and trunk of Tübingen WT larvae were extracted by a suction pipette and aspirated into cold lysis buffer from Cells-to-cDNA Kit II (Ambion). Overlying yolk skin cells were dissected by fine tweezers. First-strand cDNA synthesis was performed using Sprint-RT Complete-Oligo(dT) 18 kit (Clontech). cDNAs were amplified by PCR using ChoiceTaq Blue Master Mix (Denville Scientific) with primer pairs targeting *cadherin23* (forward, 5′-cagtagttgcaggctccaca-3′; reverse, 5′-tgggctgctaactccagatt-3′), *rbc3α* bp 8726-9105 (forward, 5′-gcagcagttgatcatcacgggcggcaggaaggg-3′; reverse, 5′-gaggatctggaatatactggccggaatgttgtagcggtcggg-3′), *rbc3α* bp 8913–3′ UTR (forward, 5′-catggcctcatgcactcattcagcacc-3′; reverse, 5′-cgtggggcgaggtgcgagata-3′), or *atp6v1aa* bp 748–1299 (forward, 5′-ggagccttcggctgtggcaag-3′; reverse, 5′-ccagaacacctgcacaatac-3′). Water was used as a negative template control.

Video monitoring of the auditory escape behavioral response. Larvae at 5 dpf were placed in 200 μl of E3 buffer in standard translucent 96-well microplate (Corning Life Sciences). The plate was vibrated by a Type 4810 shaker (Brüel & Kjær) in the dark inside a Zebrabox monitoring system (ViewPoint Life Sciences). Pure-tone stimuli delivered by the shaker were generated with VideoTrack version 3 software (ViewPoint Life Sciences) and amplified by STR-DG510 sound system (Sony). Sound pressures (SPL) were determined by placing a hydrophone (WP-23502-P16; Knowles Electronics) at the bottom of each well and recording voltage amplitudes with a TDS 1002B oscilloscope (Tektronix). Voltages were then compared with an acoustic calibrator at 94 dB and 1 kHz in air, which converted to 120 dB under water using 1 μPa as reference pressure (model 521; AcoPacific). Stimuli were presented for 100 ms at 1 kHz with pressure levels of 132, 138, or 146 dB. Behavioral responses were recorded using a Dragonfly2 Camera CCD (Point Grey Research) and binned into 1 s timeframes with the VideoTrack software. Camera and VideoTrack settings were as follows: 100 ms shutter speed, 10 dB gain, 10 fps frame rate, 12 pixels detection sensitivity, 50 pixels burst activity threshold, and 10 pixels freeze behavior. An infrared light source continuously illuminated the larvae. For quantification of the auditory escape behavioral response (AEBR), six trials were performed per larvae ($n \geq 24$ animals per genotype) with 3 min of rest between trials at each sound pressure level. Response percentages were calculated as the average for six trials. A response was scored as positive if an animal generated burst activity above a 50 pixel change. Spontaneous movement was recorded 2 s before the stimulus. The percentages of spontaneous movement were as follows: WT, 6.9%; *rbc3α*^{Q850X}, *rbc3α*^{Y2056X}, and *rbc3α*^{Y2449X}, 1.4%.

High-speed video capture of AEBR. Larvae *rbc3α*$^{+/Q850X}$ and *rbc3α*$^{Q850X/-}$ at 5 dpf were placed in a standard Petri dish filled with E3 buffer. AEBRs induced by a light tap generated by the researcher to the side of a dish were imaged using a FASTCAM PCI512 high-speed CCD camera (Photron). Images were captured at 1000 fps (512 × 512 pixels). Several larvae ($n = 5$ each genotype) were imaged simultaneously on a Carl Zeiss Axiovert 100 microscope and analyzed by NIH ImageJ software.

Primary antibodies for immunohistochemistry and fluorescence labeling. Rabbit polyclonal pan-MAGUK (1:500 dilution) and mouse monoclonal Ribeyeb (1:1000 dilution) antibodies were described previously (Sheets et al., 2011). Rabbit polyclonal Vglut3 antibody (1:1000 dilution) was described previously (Obholzer et al., 2008). Atp6V1A (a and b) proteins were targeted by rabbit polyclonal antibody, 1 μg/ml dilution (17115-1-AP; Proteintech Group). Pan-Rab3 mouse antibody (1:1000 dilution; catalog #107011; Synaptic Systems). Actin was labeled by incubation with Alexa Fluor 488–phalloidin (1:1000 dilution; Invitrogen).

Whole-mount immunohistochemistry and fluorescent imaging. Zebrafish larvae at 5 dpf were fixed in 4% paraformaldehyde and PBS with 0.02% Tween (PBS-T) overnight at 4°C, permeabilized with ice-cold acetone for 5 min, and blocked with PBS-T containing 1% bovine serum albumin and 1% dimethylsulfoxide for 2 h room temperature. They were then incubated with primary antibodies in blocking buffer overnight at 4°C, washed several times in PBS-T, and incubated in blocking buffer with secondary antibodies conjugated to Alexa Fluor 488 (Invitrogen) and *DyLight 549* (Jackson ImmunoResearch). Images through the *Z*-plane were collected with a Carl Zeiss Axiovert ImagerM.1 microscope with an LSM700 confocal scan head, Axiocam MrM camera, oil-immersion lens Carl Zeiss Plan Apochromat 63×/1.4 numerical objective (Carl Zeiss). Laser lines at 488 and 555 nm were used for excitation, and laser intensities were adjusted to minimize photobleaching.

For quantification of the Atp6V1A (a and b), neuromasts IO1-3 and SO1-3 were used because of their exceptional preservation of morphology of the hair bundles after paraformaldehyde fixation. Top-down confocal images were collected through the *Z*-plane of the entire neuromast (10–15 μm). Statistical subtraction was then performed with MetaMorph software (Molecular Devices) with a threshold set to 300 pixels. Single optical sections of 1 μm that were beneath the apical hair bundle were selected for analysis of apical compartments. Maximum *Z*-plane projections of the basal end (3 μm optical section) were selected for basal measurements. Total neuromast V1A signal was measured for maximal projections through the *Z*-plane of the entire neuromast.

For quantification of the Rab3 and Vglut3 signal, L2 neuromasts were used for confocal microscopy. Maximal *Z*-projections of the entire neuromast were performed (10–15 μm). Statistical subtraction was performed, and neuromasts were thresholded to 150 pixels and measured. For determination of Ribeyeb and pan-MAGUK overlap, Manders correlation coefficients were determined for maximal *Z*-projections of L2 neuromasts using the plugin JACob of NIH ImageJ (Bolte and Cordelières, 2006).

Live-cell imaging. For live imaging, larvae at 5 dpf were anesthetized in 0.01% tricaine and embedded in 1.5% low-melt agarose containing tricaine. Live-cell staining was performed with confocal microscopy using a water-immersion lens 60×/0.95 numerical aperture objective. Laser lines at 488 and 555 nm were used for excitation. The entire neuromast was imaged for analysis with NIH ImageJ. Hair cells that displayed very high expression of transgene constructs, including aberrant nuclear signal, were excluded from additional analysis.

LysoTracker staining of acidic compartments. LysoTracker DND-99 dye (Invitrogen) at 100 nM concentration was used for labeling acidic compartments. Larvae were continuously incubated with dye and then imaged (555/590 nm excitation/emission). *Z*-stacks of L2 neuromasts were used for comparison. Images were thresholded to 100 and measured with NIH ImageJ. LysoSensor GREEN-DND-189 (Invitrogen) was added at 100 nM[SCAP], and emission was imaged at 505 nm.

V-ATPase pharmacological inhibition. Bafilomycin A1 inhibitor (Sigma) was added to the whole-larvae bath at a final concentration of 1 μM. Larvae were incubated for 5 min and washed repeatedly before imaging.

Electrophysiology and lateral-line afferent recordings. Our recording setup for both microphonics and action currents has been described previously (Obholzer et al., 2008; Trapani and Nicolson, 2010). To suppress muscle activity, larvae were anesthetized and then microinjected in the heart with 125 μM α-bungarotoxin. For extracellular current recordings, borosilicate glass pipettes were pulled (P-97; Sutter Instruments) with a long taper and had resistances between 5 and 15 MΩ in extracellular solution. Microphonic electrodes resembled standard patch pipettes with resistances from 1 to 5 MΩ in extracellular solution. Signals were obtained using an EPC 10 amplifier and Patchmaster software (HEKA). Extracellular action currents were recorded from the soma of an individual lateral-line afferent neuron with seal resistances ranging from 20 to 80 MΩ. The recordings were done in voltage-clamp mode, sampled at 50 μs/pt, and filtered at 1 kHz. Microphonic potentials were performed in current-clamp mode and sampled at 100 μs/pt. An additional amplifier (model 440; Brownlee Precision) was used for a total of 10,000× gain and 50 Hz filter of the voltage signal. For microphonics, the recording electrode was positioned (MPC-385; Sutter Instruments) adjacent to the neuromast at the height of the hair-cell stereociliary bundles. For action current recordings, the electrode was positioned within the posterior lateral-line ganglion. The neuromast innervated by the selected afferent neuron was then identified by incrementally moving the water jet from neuromast to neuromast until phase-locked spiking was seen in response to stimulation of the innervated neuromast.

Mechanical stimulation. Stimulation of neuromast hair cells was performed with a pressure clamp (HSPC-1; ALA Scientific) attached to a glass micropipette (~30 μm tip diameter) filled with extracellular solution. The water-jet pipette was positioned (MP-265; Sutter Instruments) ~100 μm from a given neuromast, and displacement of the kinocilia was verified by eye.

Signal analysis. Data were analyzed using custom software written in Igor Pro (Wavemetrics) and were plotted with Prism 5 (GraphPad Software). Average spike rate (spikes per second) was computed from the total number of spikes in 60 consecutive 1 s traces. Average spike latency from the start of each cycle and the degree of synchrony between the stimulus wave and the action current response (calculated as vector strength) was performed as described previously (Trapani et al., 2009). Representative microphonic traces were the average of 200 consecutive 500 ms traces. Mean power spectral density (PSD) was then determined from the sum of individual PSDs for each of the 200 traces during the 200 ms stimulus portion of each trace.

Statistical analysis. Average data are presented as the mean ± SEM. Statistical significance was determined using a Student's two-tailed *t* test (paired or unpaired as appropriate), Mann–Whitney test, or ANOVA (one-way ANOVA with Bonferroni's multiple comparisons test). Differences between groups were considered significant if p values were <0.05. Statistical analyses were performed and graphs were constructed using Prism 5.0 software.

Results

Hearing, balance, and vision are impaired in *stardust/rbc3α* mutants

As part of the Tübingen 2000 Screening Consortium, we screened >1000 F2 families for mutants with balance and hearing defects to identify genes required for auditory/vestibular function in zebrafish. Five recessive alleles of a gene we named *stardust* were identified by complementation analysis. One line did not survive after several generations and was not further characterized. Mutant *stardust* larvae are morphologically normal and do not display any obvious degeneration or necrosis. Mutant larvae perform an escape response to either touch stimuli or acoustic stimuli produced by tapping on the tank or Petri dish. However, during the escape response, mutants have an aberrant body-axis orientation while swimming and fail to maintain an upright position. In addition, they do not inflate their swim bladder and lack spontaneous eye movements, and their melanocytes do not contract when exposed to bright light (data not shown). Collectively, these responses suggest that both the visual and vestibular systems are impaired in *stardust* mutants.

To understand the contribution of *stardust* to detection of sensory stimuli, we measured the AEBR, which is a simple and well-defined behavior (Nicolson et al., 1998; Zeddies and Fay, 2005). Using a high-speed video camera, we first inspected the swimming and turning behaviors during the escape response to an acoustic tap stimulus. We compared multiple still frames of the escape reflex of 5 dpf WT siblings and homozygous *stardust* mutants carrying the putative strong allele, $rbc3\alpha^{Q850X}$ (see positional cloning below). At rest, WT larvae were oriented dorsal side up with respect to gravity, whereas $rbc3\alpha^{Q850X}$ mutants were supine on the bottom of the dish with their ventral side exposed (Fig. 1*A*; $n = 5$ each). This lack of an upright position is similar to the postural defects seen in other balance-defective mutants (Nicolson et al., 1998). In response to a tap stimulus, WT and mutant larvae performed C-bends or counter turns and then swam several body lengths away (>3.5 mm). After short bouts of swimming, the WT larvae resumed a dorsal upright position, whereas the mutants were lying on their sides. These coordinated motor behaviors indicate that WT and mutant larvae are capable of performing an escape response, despite the obvious vestibular deficits in the mutants.

The presence of an escape response to loud, multispectral stimuli (tapping) does not exclude the possibility of a more subtle defect in hearing. We therefore assessed the auditory system in *stardust* mutants by testing the AEBR to either tap stimuli or pure tones delivered at a given sound pressure. WT siblings and $rbc3\alpha^{Q850X}$, $rbc3\alpha^{Y2056X}$, or $rbc3\alpha^{Y2449X}$ larvae were placed in in-

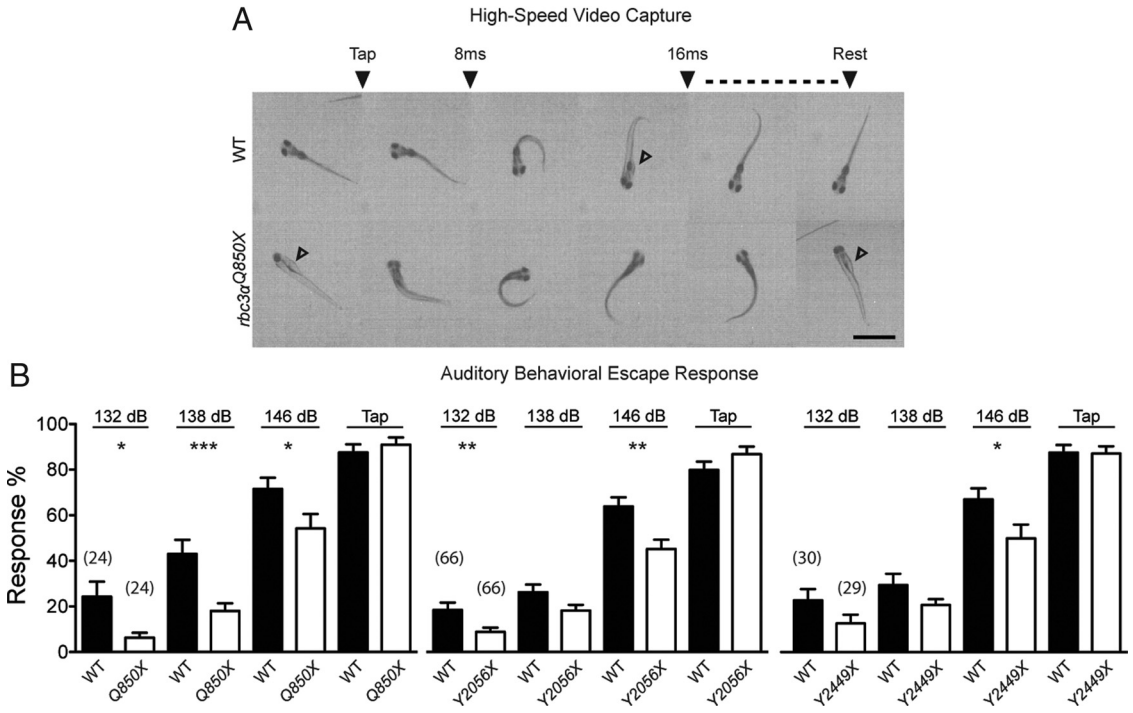

Figure 1. Homozygous *stardust/rbc3α* mutants have auditory and vestibular deficits (5 dpf). ***A***, High-speed video capture of a WT and mutant $rbc3\alpha^{Q850X}$ larvae escape response to an acoustic tap. Scale bar, 2 mm. Arrowheads denote exposed ventral side of larvae. ***B***, Quantification of escape responses in larvae exposed to either a tap or 1 kHz frequency tone at 132, 138, and 146 dB ($n \geq 24$). Error bars represent SEM, $^*p < 0.05$, $^{**}p < 0.01$, $^{***}p < 0.001$. Numbers in parentheses above histogram bars represent the number of larvae tested.

dividual wells of a 96-well plate in the dark. The percentage of larvae that performed an AEBR to a tap stimulus was not significantly different between WT and $rbc3\alpha^{Q850X}$, $rbc3\alpha^{Y2056X}$, or $rbc3\alpha^{Y2449X}$ animals (Fig. 1*B*; $n \geq 24$ animals each; $p > 0.05$, unpaired Student's *t* test). As stated previously, the response to a tap stimulus confirmed that mutant larvae were capable of generating a startle response. Next, we tested pure tones and chose sound pressures ranging from 132 to 146 dB at a frequency of 1 kHz. These parameters were chosen because they yielded measureable escape responses in WT larvae and similar parameters were used in a previous study of the AEBR in zebrafish larvae (Zeddies and Fay, 2005). Because of variability in behavioral responses between strains, we limited our comparisons of WT and mutant larvae within a given strain. In contrast to the tap stimulus, at 132 dB, both $rbc3\alpha^{Q850X}$ and $rbc3\alpha^{Y2056X}$ mutants had fewer responses than WT animals ($p < 0.05$). However, mutants containing the $rbc3\alpha^{Y2449X}$ allele were not statistically different from WT animals in response. At a higher SPL of 138 dB, only $rbc3\alpha^{Q850X}$ animals had fewer responses than WT (WT, 43 ± 6%; $rbc3\alpha^{Q850X}$, 18 ± 3%, $p < 0.001$). At the highest SPL tested, 146 dB, all three mutants performed worse than WT animals (WT, 71 ± 5% and $rbc3\alpha^{Q850X}$, 54 ± 6%, $p < 0.05$; WT, 64 ± 4% and $rbc3\alpha^{Y2056X}$, 45 ± 4%, $p = 0.0013$; WT, 67 ± 5% and $rbc3\alpha^{Y2449X}$, 50 ± 6%, $p < 0.05$). The reduced AEBRs of mutant larvae indicate that hearing is impaired but not abolished. The results from this auditory test are also consistent with the observation that mutant larvae are still capable of producing a startle response.

Positional cloning, expression, and distribution of Rbc3α in hair cells

To identify the genetic lesions in *stardust* alleles, we generated a meiotic recombination map by scoring recombination events in 385 homozygous mutant larvae with microsatellite markers. A large critical interval of 3.7 Mb was defined based on the Zv8 assembly of the zebrafish genome. The critical interval contained 60 candidate genes, including *rbc3α* (also known as *dmxl2*; Fig. 2*A*). To identify lesions within candidate genes, total mRNA was reverse transcribed from extracts of homozygous larvae. We then performed PCR from amplified cDNA and sequenced amplicons from several candidates. Three alleles of *stardust* contained nonsense mutations in the gene *rbc3α* (Fig. 2*B*). A fourth allele failed to generate cDNA from *rbc3α* transcripts, but control *vglut1* transcript was detected (data not shown). Zebrafish Rbc3α is predicted to be a large protein (3065 aa), and we designated the three alleles containing stop codons according to their amino acid locations as follows: Q850X, Y2056X, and Y2449X. In contrast to many zebrafish genes, we were unable to find any duplicates of *rbc3α* in the current assembly of the zebrafish genome. Similar to its mammalian orthologs, zebrafish Rbc3α also has multiple WD-40 domains that may function as protein–protein interaction sites (Fig. 2*B*, SMARTdatabase).

To determine which tissues might contribute to the behavioral deficits of *rbc3α* mutants, we examined the expression pattern of *rbc3α* transcripts. A previous large-scale expression screen detected *rbc3α* transcripts as early as gastrulation and demonstrated wide-spread expression throughout the larval nervous system (Thisse et al., 2001). We chose to characterize developmental stages relevant to auditory startle responses. Using an RNA *in situ* probe against an internal portion of the *rbc3α* transcript, we detected transcripts in the eye, throughout the brain, and in the sensory epithelia of the ear and cranial ganglia at 3 and 4 dpf (Fig. 2*C*,*D*). The labeling seen in the inner nuclear layer and ganglion cell layer of the retina raises the possibility that mutant visual deficits may also be present at early steps in sensory detection. Although we did not detect labeling of the lateral-line organ by *in situ* hybridization, we predicted that *rbc3α* was also expressed in lateral-line hair cells. Therefore, we used RT-PCR as an alternative detection method for detection of hair-cell transcripts

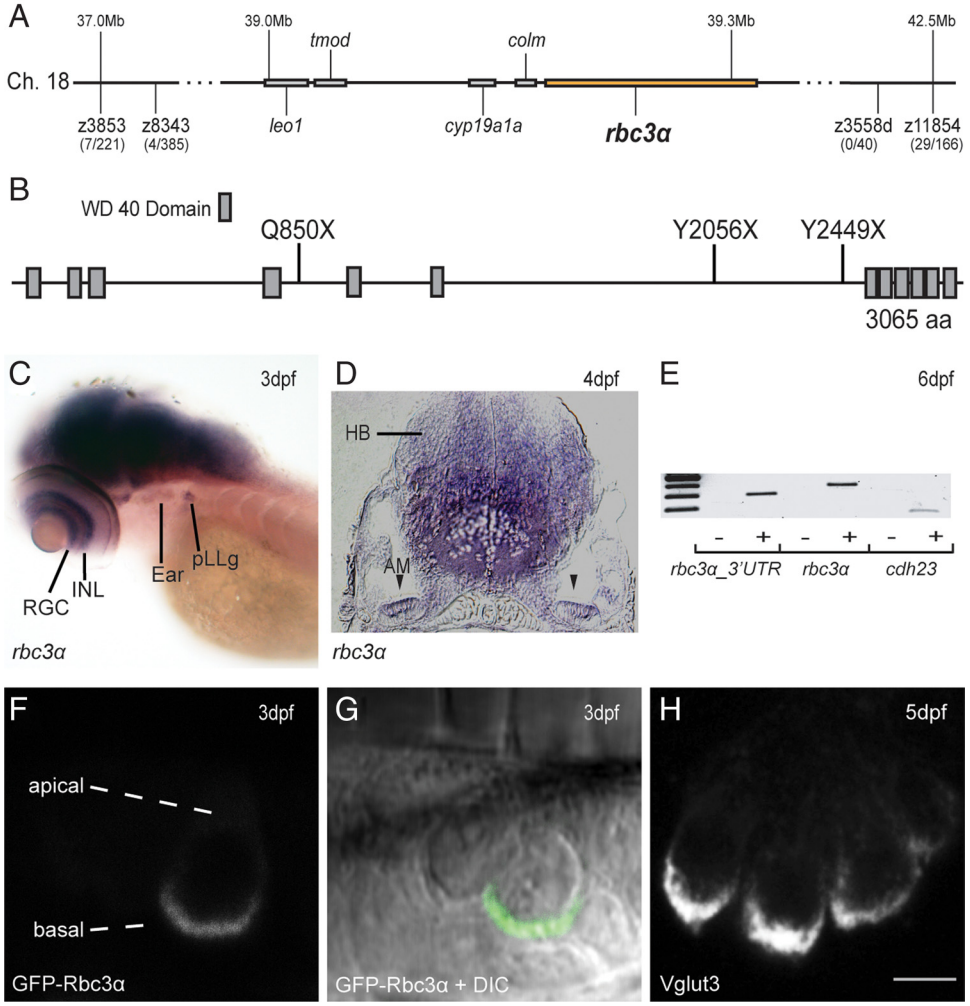

Figure 2. Positional mapping, cloning, and expression of *rbc3α*. ***A***, Map of the critical interval containing *stardust* on chromosome 18. Flanking microsatellite markers are indicated below the bar. Not all predicted genes are shown. ***B***, Three alleles of *stardust* contain nonsense mutations in *rbc3α*. The 12 predicted WD-40 repeats are indicated by gray boxes. ***C***, *In situ* hybridization pattern of *rbc3α* transcripts at 3 dpf. ***D***, A coronal section through the hindbrain and inner ear at 4 dpf stained for *rbc3α* mRNA. Arrowheads denote macular hair cells. ***E***, PCR products for *rbc3α* and hair-cell specific *cdh23* amplified using cDNA isolated from lateral-line neuromasts of WT larvae at 6 dpf. ***F***, ***G***, Confocal *Z*-projection of transient expression of *Tg(−6.5myo6b:GFP–rbc3α)* plasmid in an ampullary hair cell at 3 dpf. Rbc3α–GFP expression localized to the base of hair cells. ***H***, Example of labeling of synaptic vesicles with anti-Vglut3 antibody in inner ear hair cells (5 dpf). Scale bar, 4 μm. AM, Anterior macula; HB, hindbrain; INL, inner nuclear layer; pLLg, posterior lateral line ganglion; RGC, retinal ganglion cell.

in the lateral line (Trapani et al., 2009; Trapani and Nicolson, 2011). We isolated superficial neuromasts of larvae and prepared cDNA and then used primers against two different fragments of *rbc3α*. We amplified another known hair-cell gene, *cadherin23*, as a positive control (Fig. 2*E*). We were able to amplify *rbc3α* from neuromast cDNA (Fig. 2*E*), a result that is consistent with *rbc3α* expression in hair cells of the lateral line.

To gain a better understanding of the function of Rbc3α in hair cells, we determined whether Rbc3α is present throughout the cytoplasm or localized to subcellular regions of the hair-cell soma. We first attempted to generate specific Rbc3α antibodies but were unsuccessful. Instead, we cloned full-length *rbc3α* [GenBank accession number pending] and exogenously expressed N-terminally tagged GFP–Rbc3α in hair cells using a minimal *myosin6b* promoter. We observed that GFP–Rbc3α was localized to the basal end of hair cells in a crescent-like distribution pattern (Fig. 2*F*,*G*). The localization of GFP–Rbc3α in live cells was similar to that of Vglut3, an integral membrane protein residing within basally localized synaptic vesicles (Fig. 2*H*; Obholzer et al., 2008). The expression pattern of *rbc3α* suggests that defects in hair-cell function potentially underlie the aberrant auditory and vestibular behaviors of *rbc3α* mutants, and the localization of Rbc3α near hair-cell synapses may impart a synaptic function for the protein (Nagano et al., 2002; Sakisaka and Takai, 2005).

Rbc3α mutant hair cells fail to properly acidify synaptic vesicles

The Vglut3-like distribution pattern of GFP–Rbc3α in hair cells suggests a functional link between the protein and synaptic vesicles. Previous genetic evidence also argues for the importance of Rbc3α in the acidification of other intracellular compartments (Yan et al., 2009; Sethi et al., 2010). Therefore, we predicted that the loss of Rbc3α would also affect synaptic vesicle acidification. To examine this possibility, we applied the pH-dependent and cell-permeant dye LysoTracker to whole larvae to label acidic compartments. LysoTracker has been used to examine synaptic vesicles in retinal bipolar termini (Abreu et al., 2008). In live hair cells of WT larvae, the dye readily accumulated at the basal end of hair cells in which synaptic vesicles reside (Fig. 3*A*,*B*). Interestingly, at lower-gain settings, ring-like topologies or tori at the base of the hair cell became apparent (Fig. 3*A*). To determine whether LysoTracker dye labeled acidic synaptic vesicles sur-

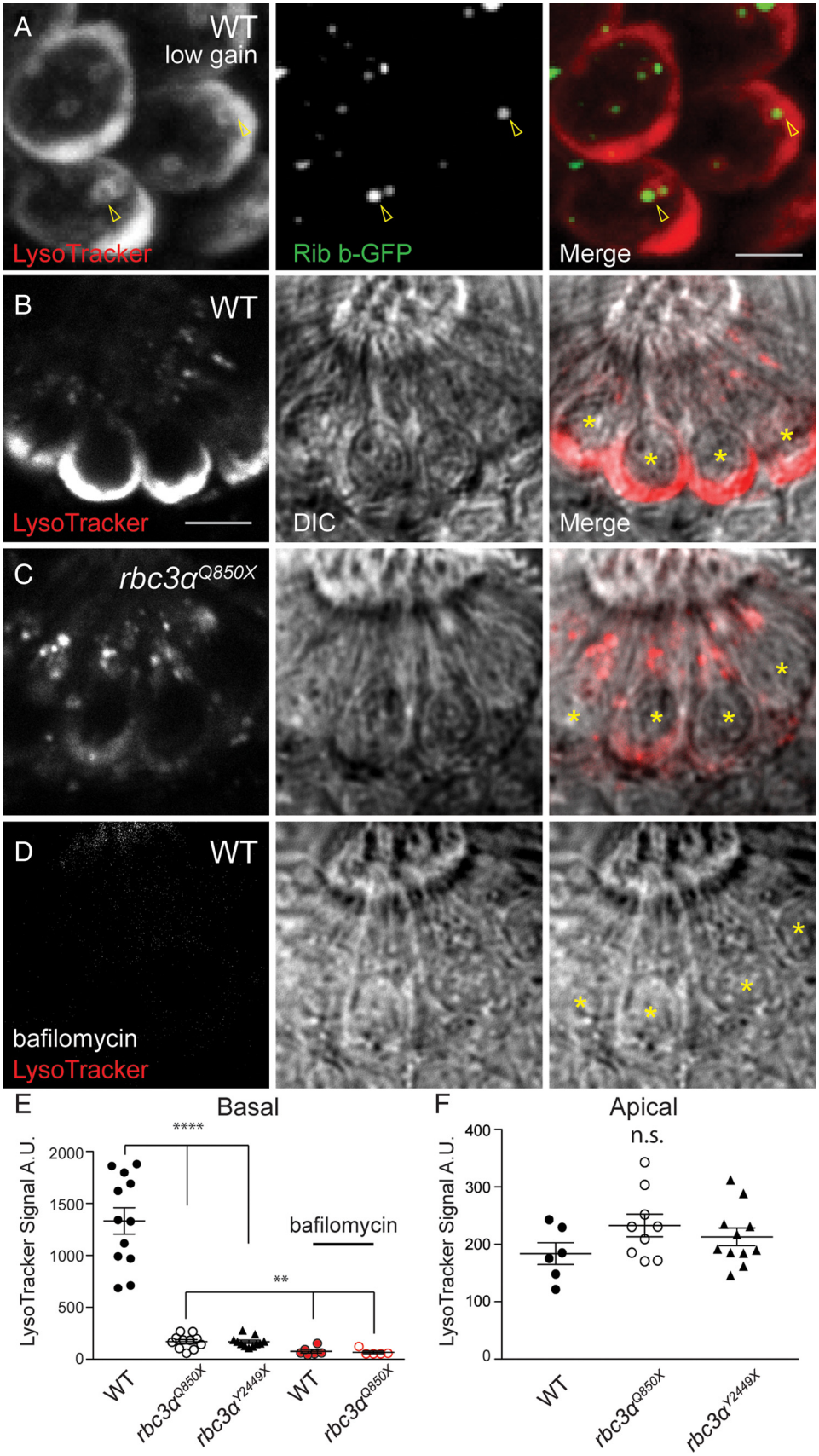

Figure 3. Rbc3α is required for proper acidification of basal vesicles. ***A***, Confocal image of a $WT^{Tg(-6.5kb\_myo6b:Ribeye\ b\text{-}GFP)}$ lateral-line L2 neuromast labeled with LysoTracker vital dye. Arrowheads indicate Ribeye b–GFP puncta and surrounding synaptic vesicle pool. Top-down view of hair cells and low gain were used to visualize tori. Scale bar, 2 μm. ***B***, ***C***, (*Figure legend continues*.)

rounding each ribbon body, we applied the dye to transgenic larvae stably expressing Ribeye b–GFP. The Ribeye b–GFP aggregates were surrounded by the LysoTracker-labeled tori, confirming that ribbon-associated vesicles were labeled. In addition, immunolabel of Vglut3 also surrounds Ribeye b-positive puncta (data not shown; Obholzer et al., 2008). We next examined live hair cells of mutant larvae to determine whether hair cells require Rbc3α for synaptic vesicle acidification. For comparison between genotypes, we restricted our analysis to neuromasts at the same position (L2) along the trunk. Basal LysoTracker signal of either *rbc3α*^{Q850X} or *rbc3α*^{Y2449X} mutants was greatly reduced compared with WT hair cells but not between alleles [Fig. 3*B*,*C*,*E*; WT, 1332 ± 126 arbitrary units (A.U.), $n = 12$; *rbc3α*^{Q850X}, 169 ± 20 A.U., $n = 11$; *rbc3α*^{Y2449X}, 168 ± 15 A.U., $n = 11$; one-way ANOVA; $F_{(2,31)} = 74.8$; $p < 0.0001$]. A similar observation of reduced LysoTracker signal was made for the mutant *rbc3α*^{Y2056X} (data not shown). In addition, the fluorophore LysoSensor GREEN-DND-189 (LysoSensor) has been used to label phagosomes in microglia of zebrafish (Peri and Nüsslein-Volhard, 2009). We found that it also labels synaptic vesicles in WT hair cells more readily than mutant hair cells (data not shown). The maximal emission of LysoSensor is greatest at pH 4–5, suggesting that mutant synaptic vesicles have elevated pH. Together, these results indicate that proper synaptic vesicle acidification requires functional Rbc3α.

The residual labeling of mutant synaptic vesicles suggested that low levels of V-ATPase activity were still present. Therefore, to determine whether Rbc3α acts as a modulator of V-ATPase activity, we then applied the V-ATPase-specific inhibitor bafilomycin to both WT and *rbc3α*^{Q850X} mutant animals. In hair cells of each genotype, basally localized LysoTracker signal was reduced to levels below that of untreated *rbc3α*^{Q850X} mutants (Fig. 3*D*,*E*; WT bafilomycin treated, 76 ± 16 A.U., $n = 6$; untreated *rbc3α*^{Q850X}, 169 ± 20 A.U., $n = 11$; *rbc3α*^{Q850X} bafilomycin treated, 64 ± 13 A.U., $n = 5$; one-way ANOVA; $F_{(2,19)} = 8.7$; $p = 0.002$). This result supports a modulatory role rather than an absolute requirement for Rbc3α in vesicle acidification. We also noted that, near the epithelial surface of hair cells, apical puncta were labeled with LysoTracker and were present in both WT and mutant hair cells. These puncta had levels that were similarly matched, suggesting that the decrease in mutant labeling was specific to basal compartments (Fig. 3*F*; WT, 183 ± 18 A.U., $n = 6$ larvae; *rbc3α*^{Q850X}, 232 ± 19 A.U., $n = 9$; *rbc3α*^{Y2449X}, 213 ± 15 A.U., $n = 11$; one-way ANOVA; $F_{(2,23)} = 1.5$; $p = 0.234$). Collectively, our results with LysoTracker suggest that the function of Rbc3α is primarily to modulate the pH of synaptic vesicles in hair cells.

Proper synaptic localization of V-ATPase subunits requires Rbc3α

Our results are consistent with a role for Rbc3α in modulating acidification of synaptic vesicles. We next set out to determine the molecular basis of this modulation. Given the interaction between various subunits of the Rbc3 complex and the V-ATPase in *Drosophila*, altered V-ATPase activity was a plausible explanation for defective acidification (Yan et al., 2009). We hypothesized that Rbc3α promotes acidification of vesicles via regulation of the proton pump. Rbc3α may influence proton pump activity in several ways, including trafficking, protein expression or degradation, or assembly of the V-ATPase holoenzyme (Toei et al., 2010).

To determine which mode of V-ATPase regulation might be affected by the loss of Rbc3α function, we examined the distributions and levels of subunits of the cytosolic (V1) and membrane (V0) sectors of the V-ATPase. To visualize the cytosolic sector, we labeled whole larvae with an anti-pan-V1A antibody and counterstained for actin using Alexa Fluor 488–phalloidin. The specificity of the V1A antibody was confirmed as ionocytes, which express high levels of V-ATPase, were robustly labeled (Fig. 4*A*,*A*′; Shiao et al., 2005; Horng et al., 2009). The V1A immunolabeling observed in hair cells was markedly enriched at basal regions in WT hair cells (Fig. 4*B*, shown in purple) but, in contrast, was evenly dispersed between apical and basal regions of *rbc3α*^{Q850X} hair cells (Fig. 4*B*′). To quantify the differences in V1A distribution between WT and mutant hair cells, we measured the ratio of apical-to-basal signal. We found that the ratio of apical-to-basal V1A signal was significantly increased in *rbc3α*^{Q850X} hair cells (Fig. 4*C*; WT, 0.54 ± 0.03, $n = 15$ neuromasts, 9 animals; *rbc3α*^{Q850X}, 0.92 ± 0.03, $n = 13$, 8 animals; $p < 0.0001$, unpaired Student's *t* test). To determine whether the increase in apical-to-basal ratio was attributable to a change in V1A expression, we measured the total fluorescence of V1A and found that the overall intensity of V1A labeling did not significantly differ between WT and mutant hair cells (Fig. 4*D*; WT, 937 ± 61 A.U., $n = 15$ neuromasts, 9 animals; *rbc3α*^{Q850X}, 889 ± 57 A.U., $n = 13$, 8 animals; $p = 0.57$, unpaired Student's *t* test). Thus, protein levels of the cytosolic V-ATPase subunit appear unaffected in mutant hair cells, whereas the distribution pattern indicates a defect in trafficking, assembly, or both.

Across species, defective assembly of the V-ATPase holoenzyme results in dispersed V1, but not V0, sectors away from normally acidified compartments (Seol et al., 2001; Smardon et al., 2002; Sautin et al., 2005). Therefore, we also examined the distribution of the membrane sector of the V-ATPase by transient expression of a GFP-tagged membrane subunit, V0A1a. Expression of GFP–V0A1a was not robust, but a few inner-ear hair cells expressed GFP–V0A1a at sufficient levels for detection *in vivo*. Unlike the altered pattern of the V1A cytosolic subunit of the V-ATPase, the distribution of the GFP-tagged membrane V0A1a was similar in both WT and *rbc3α*^{Q850X} hair cells (Fig. 4*E*,*E*′; $n = 10$ cells each). We observed higher levels of GFP signal near synaptic regions of the hair cells in both genotypes, suggesting that vesicular trafficking of the membrane V0A1a subunit is not perturbed in mutant hair cells. Normal localization of the membrane sector argues against a general trafficking defect of the proton pump.

To extend our *in vivo* analysis and confirm our findings with the pan-V1A antibodies, we also tagged a V1A subunit with GFP and examined stable transgenic expression of this cytosolic protein in live cells. In contrast to the V0A1a membrane subunit, the pattern of the cytosolic V1Aa–GFP subunit was altered in mutant hair cells. As seen with the immunolabeling experiments, WT hair cells showed an enriched GFP signal at the basal end, whereas GFP signal was dispersed in mutants (Fig. 4*F*,*F*′; WT, 0.71 ± 0.04 apical-to-basal ratio, $n = 9$ neuromasts, 9 animals; *rbc3α*^{Q850X},

←

(*Figure legend continued.*) LysoTracker labeling of L2 neuromasts in WT and mutant *rbc3α*^{Q850X} larvae at 5 dpf. ***D***, LysoTracker dye and 1 μM bafilomycin applied to a WT L2 neuromast. The oblique focal planes in ***B–D*** include the apical surface of each neuromast. Hair-cell nuclei are indicated by asterisks. Scale bar, 5 μm. ***E***, Quantification of basal LysoTracker signal. Each data point represents the average signal of an entire neuromast for WT, *rbc3α*^{Q850X}, and *rbc3α*^{Y2449X} mutants (one-way ANOVA, $F_{(2,31)} = 74.8$, ****$p < 0.0001$) and for untreated *rbc3α*^{Q850X} and bafilomycin-treated WT and *rbc3α*^{Q850X} mutants (one-way ANOVA, $F_{(2,19)} = 8.7$, **$p = 0.002$). Mean fluorescent signals were significantly different between WT and mutant neuromasts. ***F***, Quantification of apical LysoTracker staining for WT, *rbc3α*^{Q850X}, and *rbc3α*^{Y2449X} (one-way ANOVA, $F_{(2,23)} = 1.5$, $p = 0.234$). DIC, Differential interference contrast.

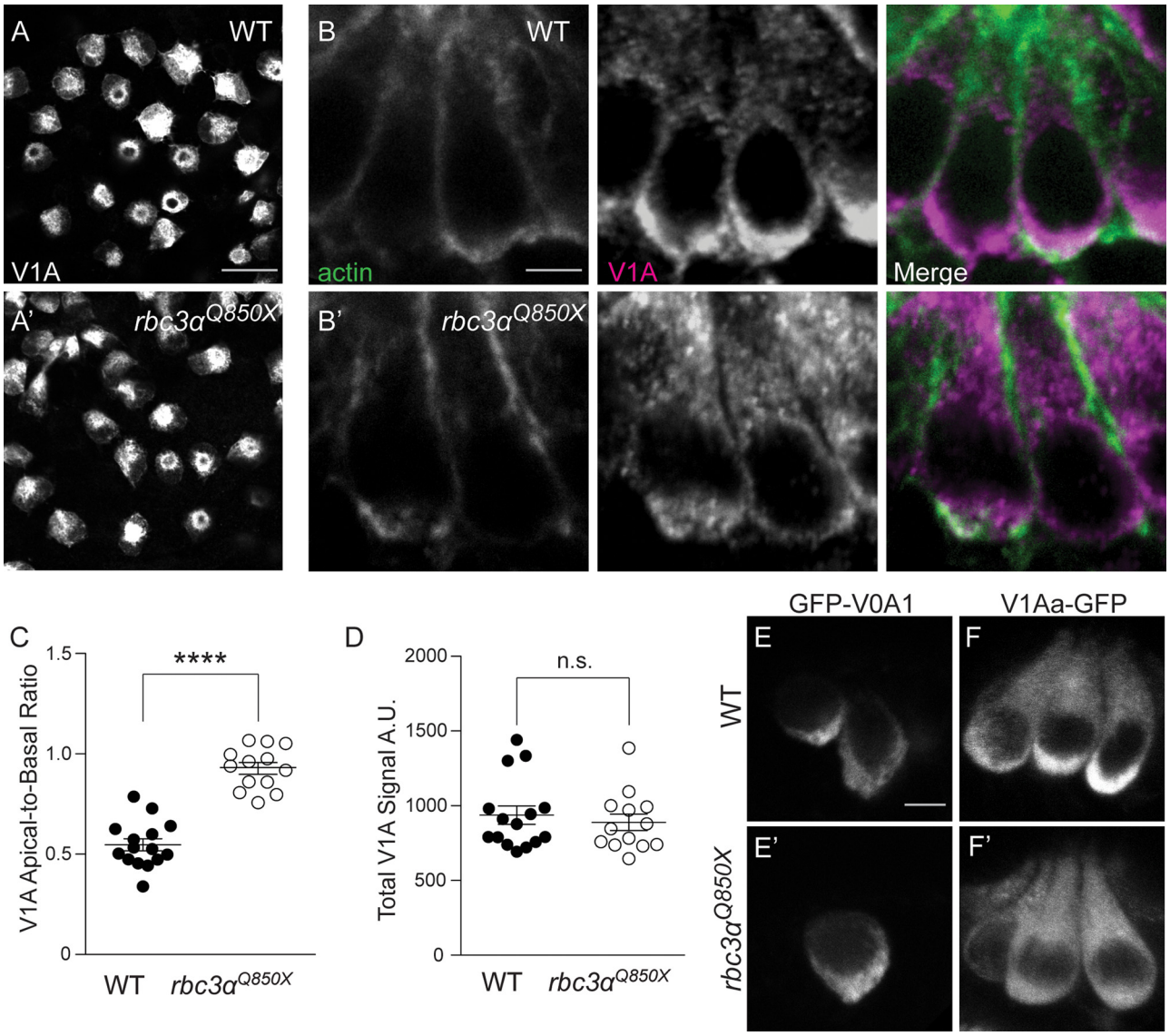

Figure 4. Cytosolic V1 sectors are redistributed in *rbc3α* mutants. ***A***, ***A′***, Positive control for Atp6V1A immunolabeling (V1Aa and V1Ab cytosolic subunits) of yolk ionocytes in WT and mutant larvae. Scale bar, 20 μm. ***B***, ***B′***, Side view of WT and *rbc3α*^{Q850X} lateral-line hair cells labeled with Alexa Fluor 488–phalloidin and V1A antibody. Labeling of V1A cytosolic subunits was enhanced at the base of WT but not mutant hair cells. Scale bar, 3 μm. ***C***, Enhanced apical-to-basal ratio of V1A immunofluorescent signal in *rbc3α*^{Q850X} mutants (WT, $n = 15$ neuromasts, 9 animals; *rbc3α*^{Q850X}, $n = 13$, 8 animals; **** $p < 0.0001$, unpaired Student's *t* test). ***D***, Average V1A fluorescent signal of whole neuromasts (WT, $n = 15$ neuromasts, 9 animals; *rbc3α*^{Q850X}, $n = 13$, 8 animals; $p = 0.57$, unpaired Student's *t* test). ***E***, ***E′***, Transient expression of V0a1 subunit using *Tg(myo6b:GFP–Atp6V0A1a)* plasmid in ampullary hair cells at 3 dpf. Note strong basal signal in both WT and mutant hair cells. ***F***, ***F′***, Stable transgenic expression of V1Aa subunit in *Tg(myo6b:GFP–Atp6V1Aa)* larvae. Side view of L2 neuromast at 5 dpf. Note stronger basal signal in WT (***F***) than mutant (***F′***) hair cells (WT, $n = 9$ neuromasts, 9 animals; *rbc3α*^{Q850X}, $n = 5$ neuromasts, 5 animals; $p = 0.0004$, unpaired Student's *t* test). Scale bar, 4 μm.

1.09 ± 0.06, $n = 5$ neuromasts, 5 animals; $p = 0.0004$, unpaired Student's *t* test). These findings point to a mechanism involving V-ATPase holoenzyme assembly as opposed to aberrant trafficking or protein levels in hair cells that are Rbc3α deficient.

Rbc3α may also play a role in shaping V-ATPase localization in other cell types, such as the previously mentioned ionocytes. We therefore isolated yolk epithelium, which includes numerous ionocytes, and then prepared extracts for RT-PCR of *v1aa* and *rbc3α* transcripts. We detected products for both cDNAs (data not shown), indicating that yolk epithelial cells also express the Rbc3α protein. Whereas variability in cell-to-cell labeling within individuals of both genotypes made quantification of signal intensities difficult, the loss of Rbc3α did not appear to have an obvious impact on apical V1A localization in ionocytes (Fig. 4*A*,*A′*). Consequently, pathways in ionocytes that assemble the V-ATPase holoenzyme at apical regions may have redundant mechanisms or limited need for Rbc3α. Together, these results suggest that assembly defects of the V-ATPase in *rbc3α* mutants are primarily restricted to synaptic vesicles in hair cells.

Synaptic composition is normal in *rbc3α* mutants

The distribution of the Rbc3 complex and its interaction with regulators of the small GTPase Rab3 may indicate additional synaptic roles for the complex, such as Rab3-dependent trafficking (Nagano et al., 2002; Kawabe et al., 2003). Therefore, we assessed the distributions and levels of synaptic vesicle proteins by immunolabeling hair cells with antibodies that target Vglut3 and Rab3 (a–d isoforms; Obholzer et al., 2008). We found that both Vglut3 and Rab3 were basally enriched in WT and mutant *rbc3α*^{Q850X} hair cells, and the intensity of labeling was not significantly dif-

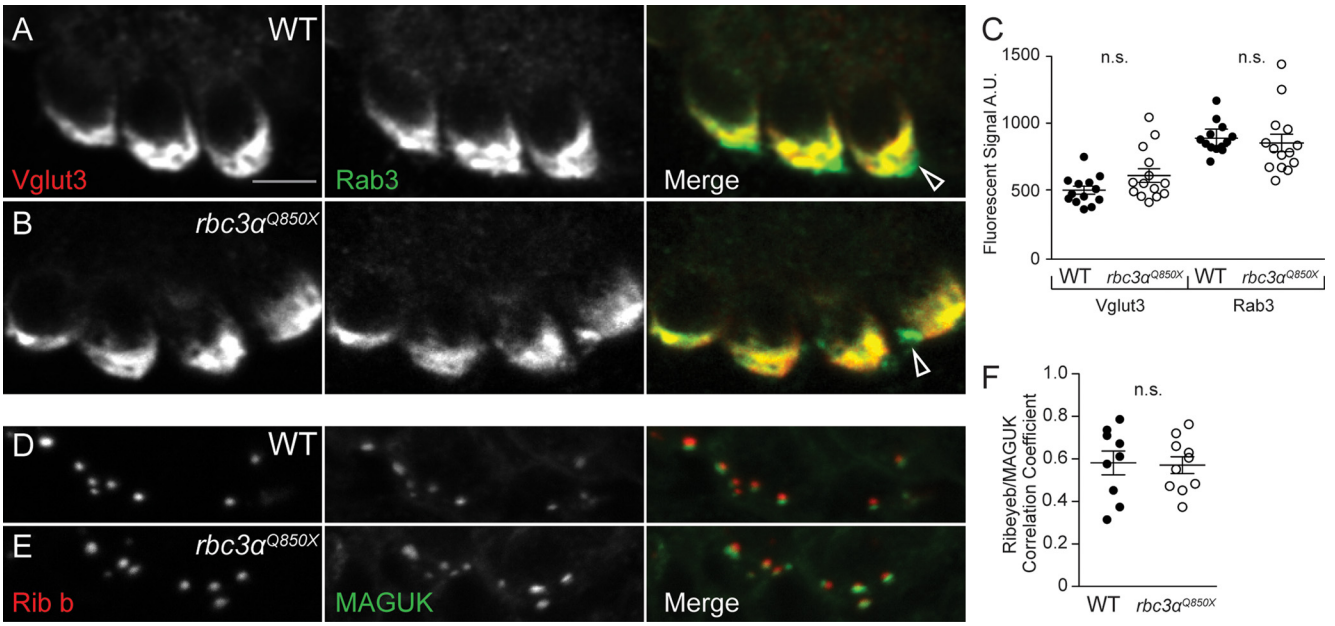

Figure 5. Loss of Rbc3α function does not affect hair-cell synaptic components. ***A***, ***B***, Confocal *Z*-projections of L2 neuromasts labeled with anti-pan-Rab3 and anti-Vglut3 antibodies in either WT (***A***) or *rbc3α*^{Q850X} (***B***) larvae at 5 dpf. Scale bar, 4 μm. Arrowheads indicate Rab3 positive efferent staining. ***C***, Quantification of immunofluorescent signal of Vglut3 ($n = 13$ neuromasts, 7 animals each; $p = 0.09$, Mann–Whitney test) and pan-Rab3 labeling ($p = 0.21$). ***D***, ***E***, Labeling of L2 neuromasts with presynaptic Ribeye b and postsynaptic pan-MAGUK antibodies. ***F***, Overlap of pan-MAGUK and Ribeye b puncta. Each data point represents the correlation coefficient of a single neuromast (Manders correlation coefficient; WT, $n = 9$ neuromasts; *rbc3α*^{Q850X}, $n = 8$ neuromasts; $p = 0.87$, unpaired Student's *t* test). Error bars represent SEM.

ferent for either proteins (Fig. 5*A*,*B*; Vglut3 WT, 496 ± 29 A.U.; mutant, 609 ± 51 A.U., $n = 13$ neuromasts, 7 animals each; $p = 0.09$, Mann–Whitney test; pan-Rab3 WT, 883 ± 31 A.U.; mutant, 856 ± 62 A.U.; $p = 0.21$, Mann–Whitney test). In addition, WT and mutant efferent termini readily labeled with Rab3 (Fig. 5*A*,*B*, arrowheads). These observations further argue against a trafficking defect or a decrease of the vesicle population.

The Rbc3 complex may also play a role in the synaptic development of the lateral line, because it is necessary for processing the intracellular domain of Notch in other organisms (Yan et al., 2009; Sethi et al., 2010), and Rab3 has been implicated in the nucleation of the neuromuscular junction in *Drosophila* (Graf et al., 2009). We therefore labeled presynaptic ribbon bodies with an anti-Ribeye b antibody and labeled postsynaptic contacts with an antibody against MAGUK proteins (Fig. 5*D*,*E*; Sheets et al., 2011). We observed that *rbc3α*^{Q850X} mutants and WT hair cells contained Ribeye b- and MAGUK-positive puncta with similar colocalization of both proteins (Fig. 5*F*; Manders correlation coefficient, WT, 0.58 ± 0.05 $n = 9$; *rbc3α*^{Q850X}, 0.57 ± 0.04, $n = 8$; $p = 0.87$, unpaired Student's *t* test). We also did not observe obvious morphological defects or cell death within the inner ear or neuromasts. Altogether, our observations suggest that the contribution of Rbc3α to the mutant auditory and vestibular behavioral phenotypes is not attributable to an obvious disruption in the development or morphology of hair-cell synapses.

Synaptic activity is reduced in *rbc3α* mutants

Hair cells transduce high-frequency stimuli with temporal precision that is maintained during sustained periods of stimulation (for review, see Nouvian et al., 2006). To support high rates of neurotransmitter release, a hair cell must ensure that synaptic vesicles are sufficiently acidified for optimal filling of neurotransmitter. Considering the defective acidification of synaptic vesicles in *rbc3α* mutants, we hypothesized that reduced V-ATPase activity would result in reduced synaptic transmission at mutant hair-cell synapses. In addition to reduced release of neurotransmitter, it was not clear whether mechanotransduction would also be sensitive to changes in apical V-ATPase activity (Shiao et al., 2005; Wangemann, 2006). To determine whether reduced V-ATPase activity had any effect on mechanotransduction, we first recorded microphonic potentials in the presence of bafilomycin. Drug treatment did not have an obvious effect on microphonic potentials (data not shown). Consistent with this observation, the amplitude and power spectra of the microphonic potentials were similar in response to 20 Hz stimulation of WT and *rbc3α*^{Q850X} neuromasts (Fig. 6*A*; WT, $n = 3$; mutant, $n = 6$; 20 Hz, $p = 0.24$; 40 Hz, $p = 0.93$). The absence of effect on mechanotransduction is in agreement with our previous experiments, and it suggests that the defects in *rbc3α* mutant hair cells are primarily synaptic.

In zebrafish larvae, an afferent neuron forms multiple synapses with groups of lateral-line hair cells that are all aligned with the same planar polarity in one or more neuromasts (Nagiel et al., 2008; Obholzer et al., 2008; Faucherre et al., 2009). It is not known whether single vesicles are released at each synapse during depolarization of lateral-line hair cells, as is the case for cochlear outer hair cells (Weisz et al., 2009), or whether multivesicular release occurs, as has been described for inner hair cells and bullfrog saccular hair cells (Glowatzki and Fuchs 2002; Li et al., 2009). Furthermore, in afferent neurons of mammalian inner hair cells, an EPSP at a single synapse generates a postsynaptic action potential (Rutherford et al., 2012). However, at the developmental stage used for our recordings, the action potentials of a single afferent neuron are generated after activation of potentially many more synapses. Thus, it is not known whether a single EPSP is sufficient or whether EPSPs from multiple synapses must summate to bring the afferent neuron to threshold in the lateral line.

To examine synaptic transmission of WT hair cells and *rbc3α* mutant hair cells, we recorded evoked action potentials from afferent neurons of the lateral-line organ. First, we confirmed our

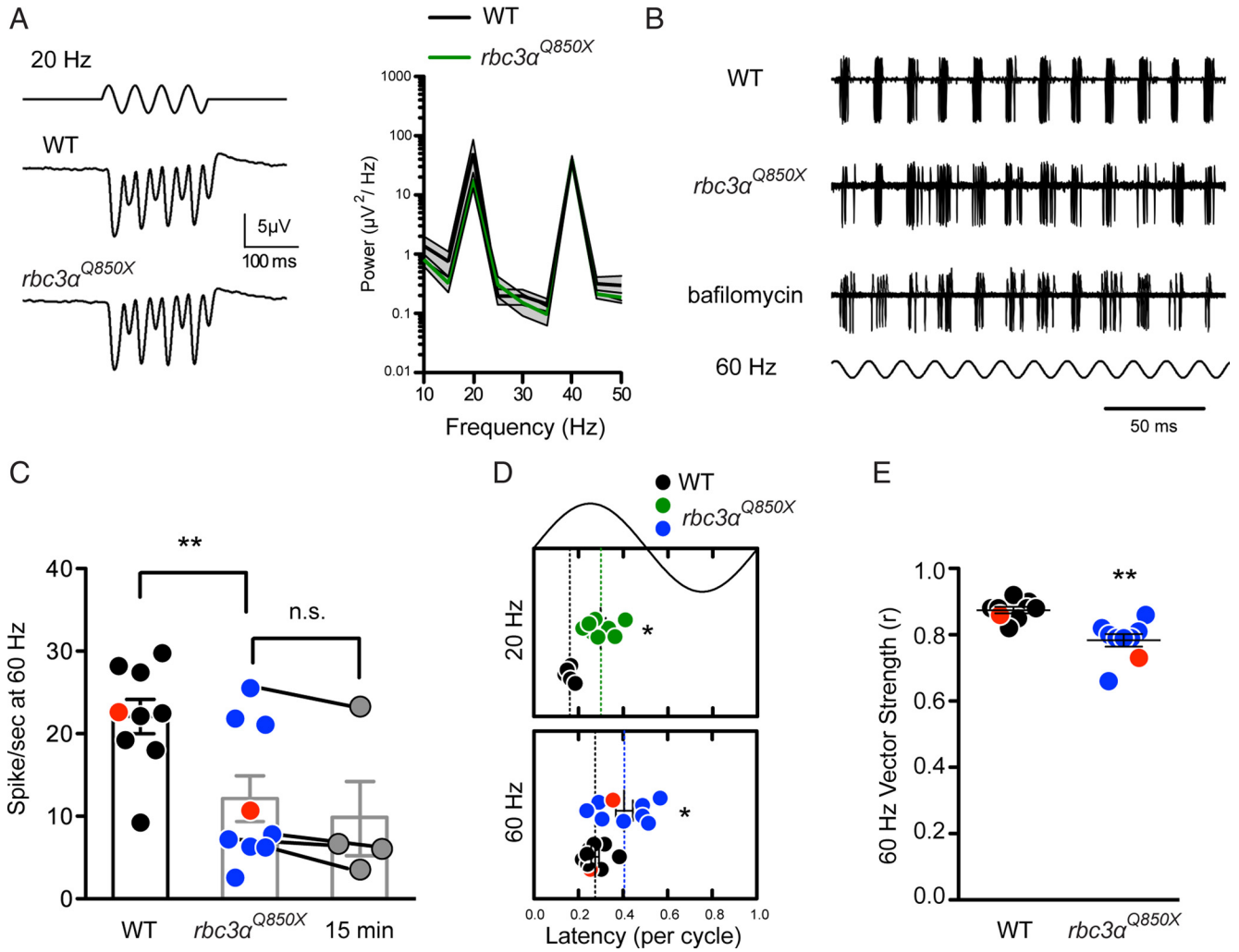

Figure 6. The rate and fidelity of stimulus-dependent spiking of lateral-line afferent neurons is reduced in *rbc3α* mutants. ***A***, Left, Average microphonic potentials recorded from WT (middle) and mutant (*rbc3α*^{Q850X}; bottom) larvae in response to 20 Hz stimulation for 200 ms (top). Right, Comparison of power spectra from microphonic potentials recording during the stimulus presentation from WT ($n = 3$) and *rbc3α*^{Q850X} ($n = 6$) larvae for frequency components between 10 and 50 Hz. Note the large peaks at both the stimulus frequency (20 Hz) and the 2f frequency, 40 Hz. Error is represented by gray shaded area above and below solid lines. ***B***, Traces of spikes recorded from afferent neurons during stimulation of hair cells at 60 Hz. Each panel is an overlay of 60 consecutive sweeps. Top, WT; middle, *rbc3α*^{Q850X}; bottom, WT treated with bafilomycin; 60 Hz stimulus waveform shown beneath the three panels. ***C–E***, The activity of afferent neurons was recorded for 60 s during either continuous 60 or 20 Hz stimulation. ***C***, Plot of the quantified average spike rate for WT (black circles), *rbc3α*^{Q850X} (blue circles), and *rbc3α*^{Q850X} after 15 min of continuous 60 Hz stimulation (gray circles). The open bars represent the mean of the recordings for each condition. ***D***, Mean latency of spikes from the stimulus deflection (positive portion of the period of a 20 or 60 Hz cycle) for recordings from WT (black circles) and *rbc3α*^{Q850X} at 20 Hz (green circles) and *rbc3α*^{Q850X} at 60 Hz (blue circles). The dashed line indicates mean latency for each condition. ***E***, The vector strength of spiking for the same recordings shown in ***C*** and ***D*** for WT (black circles) and *rbc3α*^{Q850X} (blue circles). The red symbols in ***C–E*** are from the WT and *rbc3α*^{Q850X} recordings shown in ***B***. Significance was determined by paired and unpaired Student's *t* test (as appropriate), and error bars represent SEM. $^*p < 0.05$, $^{**}p < 0.01$.

previous findings with bafilomycin by examining afferent activity during stimulation of lateral-line hair cells at 60 Hz before and during application of bafilomycin. Bafilomycin drastically reduced the firing rate of WT neurons (Fig. 6*B*; WT, 27 ± 4 spikes/s; bafilomycin, 5 ± 1 spikes/s; $n = 3$ larvae; $p < 0.05$, paired Student's *t* test). These results strongly suggest that V-ATPase activity is necessary for proper synaptic transmission, presumably by establishing the proton gradient, which provides the driving force for neurotransmitter exchange.

We next examined synaptic transmission in *rbc3α*^{Q850X} mutants by recording evoked activity of lateral-line afferent neurons from stimulating hair cells at two different frequencies: 20 and 60 Hz. At 60 Hz, the evoked firing rates of lateral-line afferent neurons were significantly reduced in *rbc3α*^{Q850X} mutants (Fig. 6*B*,*C*; WT, 22 ± 2 spikes/s, $n = 9$; *rbc3α*^{Q850X}, 12 ± 3 spikes/s, $n = 9$; $p < 0.05$, unpaired Student's *t* test). The reduced rate of spiking observed in the mutants during 60 Hz stimulation is consistent with the notion that mutant synaptic vesicles are underfilled and do not contain sufficient quantities of neurotransmitter to reliably bring the afferent neuron to threshold. In contrast to 60 Hz, stimulation at 20 Hz did not result in a significant difference between WT and mutant afferent firing rates (WT, 14 ± 4 spikes/s, $n = 5$; *rbc3α*^{Q850X}, 10 ± 3 spikes/s, $n = 7$; $p = 0.4$, unpaired Student's *t* test). Ostensibly, this difference in spiking rate at 20 versus 60 Hz in *rbc3α*^{Q850X} larvae reflects the difference in the length of the stimulus wave cycle; at 20 Hz, the 50 ms period results in a 25 ms depolarization of the hair cell, which is a longer period of time for fusion of synaptic vesicles and subsequent release of sufficient quantities of neurotransmitter. Despite normal spiking rates at 20 Hz, slower neurotransmitter release would likely result in a temporal delay to reach threshold in the afferent neuron. Indeed, there was a significant increase in the latency of firing in *rbc3α*^{Q850X} larvae at both 20 and 60 Hz when compared with WT animals (Fig. 6*D*; 20 Hz: WT, 0.16 ± 0.01, $n = 5$;

rbc3α^{Q850X}, 0.30 ± 0.02, $n = 7$; $p < 0.001$, two-tailed unpaired Student's *t* test; 60 Hz: WT, 0.27 ± 0.02, $n = 9$; *rbc3α*^{Q850X}, 0.41 ± 0.04, $n = 9$; $p < 0.01$, two-tailed unpaired Student's *t* test). The shift in latency is consistent with defective acidification and consequent reduced concentration of neurotransmitter within the synaptic vesicles of *rbc3α* mutants.

Interestingly, the effects of bafilomycin treatment had a greater effect on firing rates than the loss of Rbc3α function (Fig. 6*B*), similar to the results obtained from experiments with LysoTracker pH indicator dye (Fig. 3*D*,*E*). Furthermore, after a prolonged incubation in bafilomycin, action potentials disappeared altogether (data not shown). These results support the notion of a modulatory role for Rbc3α leading to partial filling of vesicles in the mutants in contrast to the severe depletion of neurotransmitter in vesicles after bafilomycin treatment.

The reduction in spike rate at higher frequencies would also predict that a decrease in the fidelity of stimulus encoding would be present in the mutant larvae (Wittig and Parsons, 2008). We found that the fidelity of phase-locked spiking of the afferent neuron to the 60 Hz mechanical stimulus was decreased. Calculation of vector strength, an indication of the precision of responses to a given stimulus, was significantly reduced in *rbc3α*^{Q850X} larvae (Fig. 6*E*; WT, 0.87 ± 0.01, $n = 9$; *rbc3α*^{Q850X}, 0.78 ± 0.02, $n = 9$; $p < 0.001$, unpaired Student's *t* test). We also determined the fidelity of phase locking at 20 Hz but did not observe a significant difference between WT and mutant larvae (WT, 0.96 ± 0.01, $n = 5$; *rbc3α*^{Q850X}, 0.85 ± 0.05, $n = 7$; $p = 0.13$, unpaired Student's *t* test). This result indicates that, for longer durations of stimulation such as 20 Hz cycle length, relatively normal spike rates and phase locking are still possible in *rbc3α* mutants despite a significant shift in latency.

An additional postsynaptic effect that could result from reduced release of neurotransmitter is a decrease in the rate of spontaneous spiking of the afferent neuron (Rutherford et al., 2012). We previously showed that spontaneous activity of afferent neurons in the lateral line is generated by spontaneous hair-cell neurotransmission (Trapani and Nicolson, 2011). To determine whether spontaneous activity was affected in *rbc3α*^{Q850X} mutants, we recorded afferent activity in the absence of mechanical stimulation. We observed a reduction in the rate of spontaneous action potentials in *rbc3α*^{Q850X} mutants with a significant increase in the mean interspike interval (WT, 83 ± 9 ms, $n = 11$; *rbc3α*^{Q850X}, 394 ± 141 ms, $n = 7$; $p < 0.05$, unpaired Student's *t* test).

Given that endosomes are thought to be a source for replenishing synaptic vesicles (Sudhof, 2004) and that endosomal maturation is defective in Rbc3α-deficient flies (Yan et al., 2009), we next considered whether synaptic vesicle replenishment is impaired in *rbc3α*^{Q850X} hair cells. Furthermore, like *rbc3α* mutants, a similar reduction in initial spike rate and phase locking was reported for *synj1* mutants, which have defects in synaptic vesicle recycling (Trapani et al., 2009). We therefore mechanically stimulated hair bundles with a sustained stimulus of 15 min at 60 Hz while recording the resulting evoked activity in the afferent neuron. We found that, in contrast to *synj1* mutants, sustained stimulation did not further degrade the synaptic firing rate of *rbc3α*^{Q850X} mutants (Fig. 6*C*; 10 ± 5 spikes/s; $n = 4$; $p = 0.14$, paired Student's *t* test). This result suggests that, despite the reduced rate of spiking at 60 Hz, replenishment of synaptic vesicles at this same frequency is not defective in *rbc3α*^{Q850X} hair cells. Altogether, our electrophysiology results are consistent with the synaptic defects identified by our cellular and molecular analyses, suggesting that synaptic activity is impaired as a result of deacidified and underfilled synaptic vesicles in the hair cells of *rbc3α* mutants.

Discussion

Numerous studies have demonstrated that acidification of the lumen of synaptic vesicles is a necessary step in loading neurotransmitter into vesicles (Edwards, 2007; Schenck et al., 2009; Goh et al., 2011). In this study, we demonstrate that deacidification of synaptic vesicles, by either genetic disruption of Rbc3α function or pharmacological inhibition of the proton pump, impairs synaptic transmission in hair cells. Our experiments indicate that proton gradients are reduced in mutant *rbc3α* synaptic vesicles and can be further dissipated by the proton pump inhibitor bafilomycin. Furthermore, blocking the proton pump drastically attenuates synaptic transmission in WT hair cells to levels below those in *rbc3α* mutants. Consistent with involvement of Rbc3α in synaptic vesicle acidification, the V1A cytosolic subunit of the V-ATPase was not concentrated in synaptic regions of mutant hair cells. Altogether, our data provide strong evidence for a defect in vesicle acidification that causes a reduction in the quantity of neurotransmitter in mutant synaptic vesicles. Thus, we propose that Rbc3α modulates synaptic activity in hair cells by promoting the assembly of the V-ATPase holoenzyme on synaptic vesicles, thereby regulating the internal pH of the vesicle and, ultimately, its concentration of neurotransmitter.

Several observations suggest that the primary function of Rbc3α is synaptic in nature. First, GFP–Rbc3α localizes to the basal end of hair cells in a distribution pattern akin to synaptic vesicle proteins. This distribution pattern is also in agreement with the vesicular distribution pattern observed for Rbc3α in the rat CNS (Nagano et al., 2002). Next, the acidification defect affects basally located structures, such as synaptic vesicles in mutant hair cells, whereas apical membrane compartments appear to be unaffected. Finally, various V-ATPase subunits were enriched at the basal regions of WT hair cells, whereas mutant hair cells had a pronounced decrease in the basal localization of the cytosolic subunit V1A. Similar dispersal of various V1 sector subunits has been reported for conditions causing disassembly of holoenzyme (Seol et al., 2001; Smardon et al., 2002; Sautin et al., 2005), a finding that is consistent with the notion that Rbc3α regulates synaptic vesicle acidification via a mechanism involving assembly of the cytosolic and membrane components of the proton pump.

We also considered alternative possibilities that might account for a decrease in synaptic vesicle acidification. Changes in both protein levels and trafficking of the proton pump could lead to acidification defects. However, the aberrant redistribution of V1A cytosolic subunits in mutants appeared to not be attributable to a change in V1A protein levels as evidenced by the intensity of immunolabeling. A general trafficking defect was also not apparent, because we found that subcellular localization of synaptic vesicle proteins Rab3 and Vglut3 and exogenously expressed GFP–V0A1a was unchanged in mutant hair cells. Such results are inconsistent with either degradation of proton pump subunits or a trafficking defect of the V-ATPase complex (Hurtado-Lorenzo et al., 2006; Oehlke et al., 2011).

Overall, our results point to a modulatory role for Rbc3α as opposed to an absolute requirement for synaptic vesicle acidification. Defects of vesicle acidification could be further compounded by inhibition of the proton pump with bafilomycin in the mutants. We also noted that, although the V1A cytosolic subunit appeared dispersed in mutant hair cells, its distribution still partially overlapped with the synaptic vesicle region of the

hair cell, potentially accounting for the remaining vesicular V-ATPase assembly. As mentioned previously, deacidification of synaptic vesicles would be expected to reduce neurotransmitter filling in synaptic vesicles (Edwards, 2007). Supporting this prediction, *rbc3α* mutant afferents have reduced evoked and spontaneous synaptic firing rates. In addition, there was an increased latency in spike timing and decreased phase locking of evoked action potentials in response to mechanical stimulation of hair cells. Still, the evoked firing rate of *rbc3α* mutant afferents was greater than that of WT afferents after the larvae were treated with bafilomycin. This result further suggests that mutant vesicles have partially filled vesicles attributable to the remaining V-ATPase activity.

Aside from a role in synaptic vesicle acidification, the loss of Rbc3α could also impact synaptic transmission in other ways, including perturbing vesicle trafficking or vesicle fusion. The Rbc3 complex was originally proposed to act as a synaptic scaffold on which Rab3 GEP and GAP regulate Rab3 activity (Nagano et al., 2002; Kawabe et al., 2003). Rab3 activity shapes exocytosis, Rab3-dependent cargo trafficking to the synapse, and potentially nucleation of the synapse (Tanaka et al., 2001; Niwa et al., 2008; Graf et al., 2009). Therefore, impaired Rab3 GEP and Rab3 activity might be disrupted in *rbc3α* mutants. However, the distribution of vesicular proteins Rab3 and Vglut3 and the apposition of presynaptic and postsynaptic components, Ribeyeb and MAGUK, respectively, were unchanged in *rbc3α* mutants. These findings argue against the idea that Rab3 activity is disrupted. Another possible role comes from recent evidence indicating that the V0 sector contributes to membrane fusion (Hiesinger et al., 2005; Sun-Wada et al., 2006; Peri and Nüsslein-Volhard, 2008; Di Giovanni et al., 2010). Whether synaptic vesicle fusion proceeds normally in the absence of functional Rbc3α requires additional investigation, but data from *Caenorhabditis elegans* suggests that V0-mediated membrane fusion does not require V-ATPase holoenzyme assembly (Liégeois et al., 2006).

Although the etiology resulting from the loss of V-ATPase activity in human patients is incomplete, mutations within subunits of the V-ATPase (V1B1 and V0A4) cause progressive sensorineural deafness accompanied by distal renal tubular acidosis (Karet et al., 1999; Stover et al., 2002). Assembly and trafficking of the V-ATPase in rat kidney cell lines is disrupted by mutations that mimic human V1B1 lesions in the orthologous rat V1B1 subunits, suggesting a potential mechanism behind the human disease (Yang et al., 2006). Surprisingly, however, V1B1 knockout mice are not deaf (Dou et al., 2003), suggesting that mice may have multiple mechanisms for ensuring the acidification of compartments or sub-detectable expression levels of compensatory V1B2 subunit (Finberg et al., 2005). In zebrafish larvae, various V-ATPase subunit mutations cause gross morphological defects (Nuckels et al., 2009). In contrast to the severe consequences of V-ATPase mutations, the reduced V-ATPase activity phenotype seen in *rbc3α* mutants results in a more restricted phenotype of hearing impairment in zebrafish. An explanation for the differences that we observed in the AEBR among the different *rbc3α* mutants is lacking. However, given the widespread expression of Rbc3α in the nervous system, we speculate that the neural circuitry of the escape response might be subject to differences between the alleles.

Indeed, behavioral deficits in *rbc3α* mutants are not limited to the auditory/vestibular system. Mutants also lack spontaneous eye movements and light adaptation responses in melanocytes, suggesting a possible visual defect. The selective importance of Rbc3α to visual and auditory/vestibular sensory systems, but not touch sensation, may reflect the commonalities between these tissues. Retinal bipolar cells and photoreceptors of the eye share an assortment of unique molecular specializations with the hair cell and also have ribbon-type synapses (Zanazzi and Matthews, 2009). Inherited forms of human deafness and blindness, such as Usher syndrome, are attributable to genetic lesions in the common molecular repertoire of the hearing and visual systems (hereditaryhearingloss.org). Future studies may identify synaptic defects in the retina of *rbc3α* mutants as well.

In summary, we have identified a novel role for Rbc3a in the acidification of synaptic vesicles in vertebrate hair cells. Rbc3α appears to modulate the activity of the V-ATPase holoenzyme on synaptic vesicles, most likely through a mechanism involving its assembly. Our study is the first step toward understanding how Rbc3α may act as both a synaptic vesicle scaffold and regulator of the V-ATPase.

References

Abreu BJ, Guimarães M, Uliana LC, Vigh J, von Gersdorff H, Prado MA, Guatimosim C (2008) Protein kinase C modulates synaptic vesicle acidification in a ribbon type nerve terminal in the retina. Neurochem Int 53:155–164.

Bolte S, Cordelières FP (2006) A guided tour into subcellular colocalization analysis in light microscopy. J Microsc 224:213–232.

Di Giovanni J, Boudkkazi S, Mochida S, Bialowas A, Samari N, Lévêque C, Youssouf F, Brechet A, Iborra C, Maulet Y, Moutot N, Debanne D, Seagar M, El Far O (2010) V-ATPase membrane sector associates with synaptobrevin to modulate neurotransmitter release. Neuron 67:268–279.

Dou H, Finberg K, Cardell EL, Lifton R, Choo D (2003) Mice lacking the B1 subunit of H+-ATPase have normal hearing. Hear Res 180:76–84.

Edwards RH (2007) The neurotransmitter cycle and quantal size. Neuron 55:835–858.

Faucherre A, Pujol-Mart í J, Kawakami K, López-Schier H (2009) Afferent neurons of the zebrafish lateral line are strict selectors of hair-cell orientation. PLoS One 4:e4477.

Finberg KE, Wagner CA, Bailey MA, Paunescu TG, Breton S, Brown D, Giebisch G, Geibel JP, Lifton RP (2005) The B1-subunit of the H(+) ATPase is required for maximal urinary acidification. Proc Natl Acad Sci U S A 102:13616–13621.

Fremeau RT Jr, Burman J, Qureshi T, Tran CH, Proctor J, Johnson J, Zhang H, Sulzer D, Copenhagen DR, Storm-Mathisen J, Reimer RJ, Chaudhry FA, Edwards RH (2002) The identification of vesicular glutamate transporter 3 suggests novel modes of signaling by glutamate. Proc Natl Acad Sci U S A 99:14488–14493.

Glowatzki E, Fuchs PA (2002) Transmitter release at the hair cell ribbon synapse. Nat Neurosci 5:147–154.

Goh GY, Huang H, Ullman J, Borre L, Hnasko TS, Trussell LO, Edwards RH (2011) Presynaptic regulation of quantal size: K+/H+ exchange stimulates vesicular glutamate transport. Nat Neurosci 14:1285–1292.

Graf ER, Daniels RW, Burgess RW, Schwarz TL, DiAntonio A (2009) Rab3 dynamically controls protein composition at active zones. Neuron 64:663–677.

Hiesinger PR, Fayyazuddin A, Mehta SQ, Rosenmund T, Schulze KL, Zhai RG, Verstreken P, Cao Y, Zhou Y, Kunz J, Bellen HJ (2005) The v-ATPase V0 subunit a1 is required for a late step in synaptic vesicle exocytosis in *Drosophila*. Cell 121:607–620.

Horng JL, Lin LY, Hwang PP (2009) Functional regulation of H+-ATPase-rich cells in zebrafish embryos acclimated to an acidic environment. Am J Physiol Cell Physiol 296:C682–C692.

Hurtado-Lorenzo A, Skinner M, El Annan J, Futai M, Sun-Wada GH, Bourgoin S, Casanova J, Wildeman A, Bechoua S, Ausiello DA, Brown D, Marshansky V (2006) V-ATPase interacts with ARNO and Arf6 in early endosomes and regulates the protein degradative pathway. Nat Cell Biol 8:124–136.

Karet FE, Finberg KE, Nelson RD, Nayir A, Mocan H, Sanjad SA, Rodriguez-Soriano J, Santos F, Cremers CW, Di Pietro A, Hoffbrand BI, Winiarski J, Bakkaloglu A, Ozen S, Dusunsel R, Goodyer P, Hulton SA, Wu DK, Skvorak AB, Morton CC, Cunningham MJ, Jha V, Lifton RP (1999) Mutations in the gene encoding B1 subunit of H+-ATPase cause renal tubular acidosis with sensorineural deafness. Nat Genet 21:84–90.

Kawabe H, Sakisaka T, Yasumi M, Shingai T, Izumi G, Nagano F, Deguchi-Tawarada M, Takeuchi M, Nakanishi H, Takai Y (2003) A novel

rabconnectin-3-binding protein that directly binds a GDP/GTP exchange protein for Rab3A small G protein implicated in Ca^{2+}-dependent exocytosis of neurotransmitter. Genes Cells 8:537–546.

Kwan KM, Fujimoto E, Grabher C, Mangum BD, Hardy ME, Campbell DS, Parant JM, Yost HJ, Kanki JP, Chien CB (2007) The Tol2kit: a multisite gateway-based construction kit for Tol2 transposon transgenesis constructs. Dev Dyn 236:3088–3099.

Leibovici M, Safieddine S, Petit C (2008) Mouse models for human hereditary deafness. Curr Top Dev Biol 84:385–429.

Li GL, Keen E, Andor-Ard ó D, Hudspeth AJ, von Gersdorff H (2009) The unitary event underlying multiquantal EPSCs at a hair cell's ribbon synapse. J Neurosci 29:7558–7568.

Liégeois S, Benedetto A, Garnier JM, Schwab Y, Labouesse M (2006) The V0-ATPase mediates apical secretion of exosomes containing Hedgehog-related proteins in *Caenorhabditis elegans*. J Cell Biol 173:949–961.

Mo W, Nicolson T (2011) Both pre- and postsynaptic activity of Nsf prevents degeneration of hair-cell synapses. PLoS One 6:e27146.

Nagano F, Kawabe H, Nakanishi H, Shinohara M, Deguchi-Tawarada M, Takeuchi M, Sasaki T, Takai Y (2002) Rabconnectin-3, a novel protein that binds both GDP/GTP exchange protein and GTPase-activating protein for Rab3 small G protein family. J Biol Chem 277:9629–9632.

Nagiel A, Andor-Ard ó D, Hudspeth AJ (2008) Specificity of afferent synapses onto plane-polarized hair cells in the posterior lateral line of the zebrafish. J Neurosci 28:8442–8453.

Nicolson T, Rüsch A, Friedrich RW, Granato M, Ruppersberg JP, Nüsslein-Volhard C (1998) Genetic analysis of vertebrate sensory hair cell mechanosensation: the zebrafish circler mutants. Neuron 20:271–283.

Niwa S, Tanaka Y, Hirokawa N (2008) KIF1Bβ- and KIF1A-mediated axonal transport of presynaptic regulator Rab3 occurs in a GTP-dependent manner through DENN/MADD. Nat Cell Biol 10:1269–1279.

Nouvian R, Beutner D, Parsons TD, Moser T (2006) Structure and function of the hair cell ribbon synapse. J Membr Biol 209:153–165.

Nuckels RJ, Ng A, Darland T, Gross JM (2009) The vacuolar-ATPase complex regulates retinoblast proliferation and survival, photoreceptor morphogenesis, and pigmentation in the zebrafish eye. Invest Ophthalmol Vis Sci 50:893–905.

Obholzer N, Wolfson S, Trapani JG, Mo W, Nechiporuk A, Busch-Nentwich E, Seiler C, Sidi S, Söllner C, Duncan RN, Boehland A, Nicolson T (2008) Vesicular glutamate transporter 3 is required for synaptic transmission in zebrafish hair cells. J Neurosci 28:2110–2118.

Oehlke O, Martin HW, Osterberg N, Roussa E (2011) Rab11b and its effector Rip11 regulate the acidosis-induced traffic of V-ATPase in salivary ducts. J Cell Physiol 226:638–651.

Peri F, Nüsslein-Volhard C (2008) Live imaging of neuronal degradation by microglia reveals a role for v0-ATPase a1 in phagosomal fusion in vivo. Cell 133:916–927.

Ruel J, Emery S, Nouvian R, Bersot T, Amilhon B, Van Rybroek JM, Rebillard G, Lenoir M, Eybalin M, Delprat B, Sivakumaran TA, Giros B, El Mestikawy S, Moser T, Smith RJ, Lesperance MM, Puel JL (2008) Impairment of SLC17A8 encoding vesicular glutamate transporter-3, VGLUT3, underlies nonsyndromic deafness DFNA25 and inner hair cell dysfunction in null mice. Am J Hum Genet 83:278–292.

Rutherford MA, Chapochnikov NM, Moser T (2012) Spike encoding of neurotransmitter release timing by spiral ganglion neurons of the cochlea. J Neurosci 32:4773–4789.

Sakisaka T, Takai Y (2005) Purification and properties of rabconnectin-3. Methods Enzymol 403:401–407.

Sautin YY, Lu M, Gaugler A, Zhang L, Gluck SL (2005) Phosphatidylinositol 3-kinase-mediated effects of glucose on vacuolar H+-ATPase assembly, translocation, and acidification of intracellular compartments in renal epithelial cells. Mol Cell Biol 25:575–589.

Schenck S, Wojcik SM, Brose N, Takamori S (2009) A chloride conductance in VGLUT1 underlies maximal glutamate loading into synaptic vesicles. Nat Neurosci 12:156–162.

Seal RP, Akil O, Yi E, Weber CM, Grant L, Yoo J, Clause A, Kandler K, Noebels JL, Glowatzki E, Lustig LR, Edwards RH (2008) Sensorineural deafness and seizures in mice lacking vesicular glutamate transporter 3. Neuron 57:263–275.

Seol JH, Shevchenko A, Shevchenko A, Deshaies RJ (2001) Skp1 forms multiple protein complexes, including RAVE, a regulator of V-ATPase assembly. Nat Cell Biol 3:384–391.

Sethi N, Yan Y, Quek D, Schupbach T, Kang Y (2010) Rabconnectin-3 is a functional regulator of mammalian Notch signaling. J Biol Chem 285:34757–34764.

Sheets L, Trapani JG, Mo W, Obholzer N, Nicolson T (2011) Ribeye is required for presynaptic Ca(V)1.3a channel localization and afferent innervation of sensory hair cells. Development 138:1309–1319.

Shiao JC, Lin LY, Horng JL, Hwang PP, Kaneko T (2005) How can teleostean inner ear hair cells maintain the proper association with the accreting otolith? J Comp Neurol 488:331–341.

Smardon AM, Kane PM (2007) RAVE is essential for the efficient assembly of the C subunit with the vacuolar H(+)-ATPase. J Biol Chem 282:26185–26194.

Smardon AM, Tarsio M, Kane PM (2002) The RAVE complex is essential for stable assembly of the yeast V-ATPase. J Biol Chem 277:13831–13839.

Söllner C, Schwarz H, Geisler R, Nicolson T (2004) Mutated otopetrin affects the genesis of otoliths and the localization of Starmaker in zebrafish. Dev Genes Evol 214:582–590.

Stover EH, Borthwick KJ, Bavalia C, Eady N, Fritz DM, Rungroj N, Giersch AB, Morton CC, Axon PR, Akil I, Al-Sabban EA, Baguley DM, Bianca S, Bakkaloglu A, Bircan Z, Chauveau D, Clermont MJ, Guala A, Hulton SA, Kroes H, Li Volti G, Mir S, Mocan H, Nayir A, Ozen S, Rodriguez Soriano J, Sanjad SA, Tasic V, Taylor CM, Topaloglu R, Smith AN, Karet FE (2002) Novel ATP6V1B1 and ATP6V0A4 mutations in autosomal recessive distal renal tubular acidosis with new evidence for hearing loss. J Med Genet 39:796–803.

Sudhof TC (2004) The synaptic vesicle cycle. Annu Rev Neurosci 27:509–547.

Sun-Wada GH, Toyomura T, Murata Y, Yamamoto A, Futai M, Wada Y (2006) The a3 isoform of V-ATPase regulates insulin secretion from pancreatic beta-cells. J Cell Sci 119:4531–4540.

Tanaka M, Miyoshi J, Ishizaki H, Togawa A, Ohnishi K, Endo K, Matsubara K, Mizoguchi A, Nagano T, Sato M, Sasaki T, Takai Y (2001) Role of Rab3 GDP/GTP Exchange Protein in synaptic vesicle trafficking at the mouse neuromuscular junction. Mol Biol Cell 12:1421–1430.

Thisse B, Pflumio S, Fürthauer M, Loppin B, Heyer V, Degrave A, Woehl R, Lux A, Steffan T, Charbonnier XQ, Thisse C (2001) Expression of the zebrafish genome during embryogenesis. ZFIN Direct Data Submission. Available at http://zfin.org/cgi-bin/webdriver?MIval=aa-pubview2.apg&OID=ZDB-PUB-010810-1.

Toei M, Saum R, Forgac M (2010) Regulation and isoform function of the V-ATPases. Biochemistry 49:4715–4723.

Trapani JG, Nicolson T (2011) Mechanism of spontaneous activity in afferent neurons of the zebrafish lateral-line organ. J Neurosci 31:1614–1623.

Trapani JG, Nicolson T (2010) Physiological recordings from zebrafish lateral-line hair cells and afferent neurons. Methods Cell Biol 100:219–231.

Trapani JG, Obholzer N, Mo W, Brockerhoff SE, Nicolson T (2009) Synaptojanin1 is required for temporal fidelity of synaptic transmission in hair cells. PLoS Genet 5: e1000480.

Trombetta ES, Ebersold M, Garrett W, Pypaert M, Mellman I (2003) Activation of lysosomal function during dendritic cell maturation. Science 299:1400–1403.

Wangemann P (2006) Supporting sensory transduction: cochlear fluid homeostasis and the endocochlear potential. J Physiol 576:11–21.

Weisz C, Glowatzki E, Fuchs P (2009) The postsynaptic function of type II cochlear afferents. Nature 461:1126–1129.

Wittig JH Jr, Parsons TD (2008) Synaptic ribbon enables temporal precision of hair cell afferent synapse by increasing the number of readily releasable vesicles: a modeling study. J Neurophysiol 100:1724–1739.

Yan Y, Denef N, Schüpbach T (2009) The vacuolar proton pump, V-ATPase, is required for notch signaling and endosomal trafficking in *Drosophila*. Dev Cell 17:387–402.

Yang Q, Li G, Singh SK, Alexander EA, Schwartz JH (2006) Vacuolar H+-ATPase B1 subunit mutations that cause inherited distal renal tubular acidosis affect proton pump assembly and trafficking in inner medullary collecting duct cells. J Am Soc Nephrol 17:1858–1866.

Zanazzi G, Matthews G (2009) The molecular architecture of ribbon presynaptic terminals. Mol Neurobiol 39:130–148.

Zeddies DG, Fay RR (2005) Development of the acoustically evoked behavioral response in zebrafish to pure tones. J Exp Biol 208:1363–1372.